Acta Neuropathologica Communications

RESEARCH

Open Access

Single cell protein profiling of focal cortical dysplasia in a patient requiring multiple resections

Nada A. Elsayed[1,2], Robert P. Naftel[3], Bret C. Mobley[4], Allyson L. Alexander[5,6], Angus M. Toland[7], Asa A. Brockman[2], Jonathan M. Irish[2], Rebecca A. Ihrie[2] and Kevin C. Ess[2*]

Abstract

Epilepsy affects millions worldwide with many failing to respond to standard treatments. Drug-refractory epilepsy requiring surgical intervention often presents due to developmental aberrations, such as focal cortical dysplasia (FCD). In FCD type II, somatic mutations in the mTOR pathway allow excessive activation of the mTOR kinase, causing unregulated cell growth and differentiation. Ex vivo studies of resected brain tissues offer a direct window into epileptogenic brain and disease pathophysiology. Recent studies implicate abnormal cell fate specification in FCD, but it is unclear if mutant cells are directly epileptogenic and/or whether they impact neighboring cells. Using a custom 43-antibody mass cytometry panel, we broadly assessed cell lineage and functional state across multiple sequential resections from a female child with FCD harboring a mosaic gain-of-function AKT3 mutation. Our approach used unsupervised machine learning tools to define protein-level features of dysplasia-associated cells and revealed cell populations associated with clinical outcomes. While AKT3 mutational burden did not correlate with clinical outcomes, protein profiling identified a distinct population of CUX1-high cells correlating with seizure control. Furthermore, we identified a similar cell population across multiple additional cortical malformation cases. This work demonstrates the advantage of deep single-cell protein profiling of surgically resected epilepsy tissue and provides insight on disease mechanisms that can be overlooked in traditional genetic or transcriptional studies.

Keywords AKT3, Epilepsy, Focal cortical dysplasia, Gain of function, Mass cytometry

*Correspondence:
Kevin C. Ess
Kevin.Ess@childrenscolorado.org
[1]Medical Scientist Training Program, Vanderbilt University School of Medicine, Nashville, TN, USA
[2]Department of Pediatrics, Section of Neurology, University of Colorado Anschutz Medical Campus, Aurora, CO, USA
[3]Department of Neurosurgery, Vanderbilt University Medical Center, Nashville, TN, USA
[4]Department of Pathology, Microbiology, and Immunology, Vanderbilt University Medical Center, Nashville, TN, USA
[5]Department of Neurosurgery, University of Colorado Anschutz Medical Campus, Aurora, CO, USA
[6]Division of Pediatric Neurosurgery, Children's Hospital Colorado, Aurora, CO 80045, USA
[7]Department of Pathology and Laboratory Services, University of Colorado Anschutz Medical Campus, Aurora, CO, USA

Introduction

Brain development is a highly complex process that relies on reproducible cell differentiation and signaling kinetics. Developmental aberrations can disrupt cortical structure and lead to long-term sequelae such as epilepsy and developmental delay [34]. A prime example is the heterogenous group of congenital brain malformations known as Focal Cortical Dysplasia (FCD), which is a leading cause of drug-refractory epilepsy in childhood [13]. FCD type II (FCDII) is the most common subtype and typically arises due to somatic mutations altering the mammalian target of rapamycin (mTOR) signalling pathway, placing it within a broader class of disorders termed mTORopathies. Surgical resection of dysplastic tissue can provide some therapeutic benefit to patients with FCD, although it still fails to control seizures in many patients [30]. This has led to a pressing need to better characterize mechanisms driving FCDII and subsequent epileptogenesis to improve therapeutic approaches.

FCDII is characterized histologically by abnormal cortical lamination with dysmorphic neurons (IIa & IIb) and enlarged multilineage balloon cells (IIb) [21]. Slice recordings reveal increased electrical activity in areas with a greater density of dysmorphic neurons [1], indicating they likely contribute to epileptogenesis. However, mutant cells in FCDII often make up a small proportion (< 9%) of the brain lesion [4], suggesting they exert non-cell autonomous effects on neighboring cells that are difficult to analyze through bulk approaches. This is further supported by lack of an identified genetic diagnosis in 40–70% of FCDII cases [18, 31]. Prior studies focused on elucidating mechanisms of FCD development have been limited to bulk-level protein or single-cell transcriptional analyses [5, 8, 12]. Given the potential role of low abundance cells in mediating the effects seen in FCD, it is equally important to study tissues on a single-cell level with a focus on post-translational events. Here, we use a high-dimensional mass cytometry approach to deeply phenotype thousands of individual cells in serial epileptic resections from a patient with FCD and additional unrelated malformations of cortical development (MCD) cases. Leveraging a custom-built 43-antibody panel including multiple markers of neural lineage and ten downstream phosphorylation targets of mTOR and related pathways, we uncover features of each resection that may contribute to variable therapeutic response.

Materials and methods

Human cortical tissue acquisition

The study protocol was approved by the Vanderbilt University Institutional Review Board and the Colorado Multiple Institutional Review Board. Informed consent/assent was obtained from patients and guardians. After resection, live tissue was placed in warm saline for immediate transport. Tissue was cut into three pieces for cellular dissociation, fixation, and sequencing (Fig. 2b). Dissociation tissue was processed as described below. Sequencing tissue was flash frozen. For paraffin embedding and histopathological studies, tissue was placed in 10% w/v formalin (Fisher) overnight and then transferred to 70% EtOH prior to embedding.

Tissue dissociation

Cortical brain tissue was dissociated as previously described [19]. Briefly, tissue was transferred to NeuroSphere-A (NS-A) media (StemCell Technologies), manually cut into 1 mm^3 pieces, then dissociated for 1 h at 37 °C on a rotating shaker in NS-A media with 1 mg/mL Collagenase II (Sigma-Aldrich) and 100 Kunitz units/mL DNase I (Sigma-Aldrich). After dissociation, any residual clumps were passed ~ 50 times through a 10 mL serological pipet. Dissociated cells were passed sequentially through a 100 µm and 40 µm filter (MTC Bio) to remove clumps. Cells were spun at 200 x *g* for 5 min and then resuspended in 5 mL ACK lysing buffer (Gibco) to remove residual red blood cells. After 1 min, the reaction was neutralized with 10 mL NS-A. Cells were spun at 200 x *g* for 5 min and resuspended in complete NS-A (NS-A supplemented with 0.0002% w/v heparin (StemCell Technologies), 20 ng/mL EGF (PeproTech), and 10 ng/mL FGF-2 (PeproTech)). Cells were counted using a hemocytometer, resuspended in NS-A complete with 10% DMSO (Sigma-Aldrich), and aliquoted in cryovials with 1–50 million cells/vial depending on cell count. Cells were stored in a Mr. Frosty Freezing Container (ThermoFisher) at -80 °C overnight and transferred to liquid nitrogen the next day.

Metal-conjugated antibodies

The full antibody panel is listed in Supplementary Table 1. Antibodies that were not commercially available from Standard BioTools were purchased in carrier-free formulation and conjugated using MaxPar Antibody Labeling Kits (Standard BioTools) according to manufacturer instructions. All antibodies were validated on known positive/negative controls and titrated before addition to the panel.

Cell thawing and extracellular staining

Cryovials from liquid nitrogen were quickly thawed at 37 °C. Cells were resuspended in complete NS-A and centrifuged at 200 x *g* for 5 min. Cells were stained with 250 nM Rhodium intercalator (Standard BioTools) for 5 min. Samples were quenched with 1% BSA, spun down, and transferred to 5 mL FACS tubes (Falcon) for staining with extracellular antibodies for 30 min at room temperature (Supplementary Table 1). After a brief wash,

samples were fixed for 20 min in 1.6% PFA, washed, then permeabilized with ice cold 100% methanol overnight.

Intracellular antibody staining

Samples were removed from methanol and washed twice, once with 1X PBS and once with 1% BSA. Cells were stained with three-plex 250 nM TeMal barcodes (Standard BioTools) for 15 min. After barcoding, samples were washed twice with 1% BSA then combined into one tube for intracellular staining. Samples were stained for 30 min at room temperature (Supplementary Table 1), washed with 1X PBS, then resuspended overnight in 25 nM Iridium intercalator (Standard BioTools) in 1.6% PFA. The next day, samples were acquired on the CyTOF XT (Standard BioTools).

Data analysis

Cytobank software (Beckman Coulter) was used for manual gating, debarcoding, and dimensionality reduction. Data files were gated on Gaussian parameters as previously described [28] and live cells with high Iridium and low Rhodium were used for analyses. Channels that stained well and passed quality control were used to build t-SNE maps, with specifics described in the text and Supplementary Table 1. All t-SNE maps were run over several iterations to rule out bias from down sampling across resections. Tracking Responders Expanding (T-REX) [6], Marker Enrichment Modeling (MEM) [11], and Velociraptor [9] algorithms were run using R version 4.4.1.

DNA extraction and sequencing

DNA was extracted from flash frozen tissue using the DNEasy Blood & Tissue Kit (Qiagen). DNA quantity and integrity was assessed via NanoDrop One and Qubit (ThermoFisher). 200X Whole Exome Sequencing was performed at the Genome Technology Access Center (GTAC) at Washington University in St. Louis. DNA underwent automated NGS library construction with KapaHyper amplification (Roche). Exomes were enriched using IDT exome capture. Sequencing was performed on Illumina NovaSeq X Plus with 2 × 150 paired-end reads. Samples were aligned with GRCh38 and analyzed using a DRAGEN BioIT processor running software version 4.3 in somatic mode. Variants were confirmed using Sanger sequencing.

Tissue cyclic immunostaining

Fixed, paraffin-embedded tissue specimens were sectioned and mounted on glass slides. Samples were deparaffinized with xylene. Antigen retrieval was performed at pH 6.0. Samples were stained with 20 markers over 15 cycles on the Lunaphore COMET (Supplementary Table 2). Endogenous tissue autofluorescence was subtracted from antibody-stained images using unstained autofluorescence-only controls for each fluorophore and cells of interest were manually identified.

Results

Case presentation

Our female patient was delivered at term with no complications. Her clinical course is outlined in Fig. 1. At three weeks of age, she presented to a hospital with repetitive, seconds-long, episodes of left eye deviation with occasional right upper extremity movements. Brain MRI revealed dysgyria and cortical thickening involving the left superior and medial frontal gyri (Fig. 2a – preoperative). EEG showed near continuous left-sided epileptiform discharges. She was diagnosed with presumed FCD and started on levetiracetam for seizure control. Seizures were well controlled until 23 months of age with no change after addition of oxcarbazepine. She was evaluated as a surgical candidate and later underwent stereotactic EEG (stereo-EEG) monitoring followed by surgical resection of epileptogenic foci at 32 months (Fig. 2a – resection 1). On postoperative day (POD) one, the patient had isolated seizure clusters, assumed to be due to postoperative swelling. She was discharged home but re-presented on POD5 with concerns

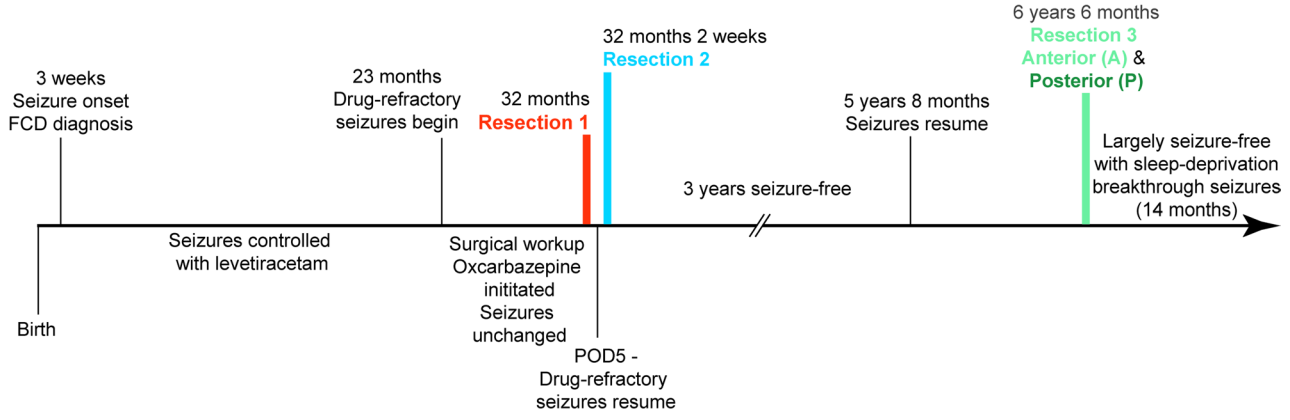

Fig. 1 Timeline of patient clinical course. POD: postoperative day

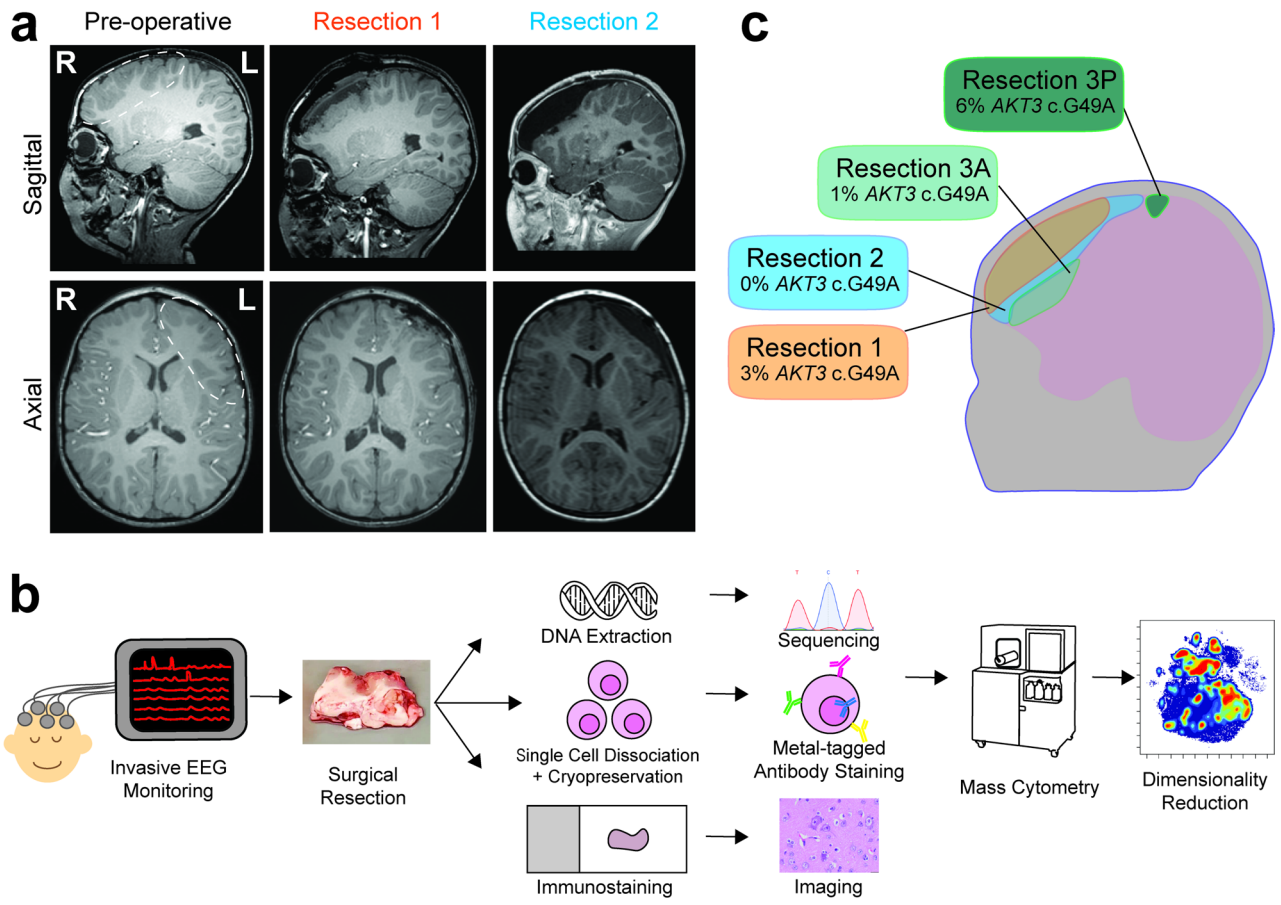

Fig. 2 A pediatric patient with well-characterized focal cortical dysplasia (FCD) required multiple surgeries for seizure control. **a** Serial MRIs depict the left frontal FCD region pre-operatively, post resection 1, and post resection 2. Resection 2 MRI was performed 3 months post-operatively. Top - Sagittal. Bottom - Axial. White dashed outlines highlight areas of dysplasia. **b** Overview of methods used to analyze patient tissue. **c** Schematic depicting *AKT3* c.G49A variant allele fractions identified in each resection with 200X whole exome sequencing, and approximate location of resection

of breakthrough seizures. EEG revealed persistent left frontal discharges. The patient underwent subdural grid electrode placement and returned to the operating room on POD14. After the second resection (Fig. 2a – resection 2), the patient remained seizure-free for 3 years. At 6 years old, the patient re-presented with seizures exhibiting a similar EEG pattern. She underwent a third resection after stereo-EEG monitoring and cortical mapping. Intraoperative electrocorticography (ECoG) revealed two distinct areas of epileptiform activity – a left frontal area (resection 3 A) with recorded seizures on stereo-EEG and a left posterior primary motor adjacent area (resection 3P) that had no activity on stereo-EEG but showed a modest frequency of epileptiform discharges during ECoG. Both areas were resected, and the patient has remained largely seizure-free to date (11 months), with some brief breakthrough seizures when sleep deprived. The patient has met all developmental milestones and has no neuropsychiatric issues.

Mutational burden does not correlate with clinical outcomes

Tissue was collected from each surgery and used for multimodal analysis (Fig. 2b). To confirm that resected tissue from each surgery met the classification of FCD, Hematoxylin & Eosin staining was performed clinically, and images were reviewed by expert neuropathologists. A diagnosis of FCDIIa was made according to ILAE classification [21], with neuronal nucleomegaly and abnormal neuronal layering and clustering present in all tissues (Supplementary Fig. 1).

Using snap-frozen tissue from each resection, we sought to identify the mutation(s) underlying this complex case. A recognized gain-of-function somatic mosaic mutation in *AKT3* (c.G49A/p.E17K) [26] was identified using whole exome sequencing with an 225x average depth of coverage (Fig. 2c). We hypothesized that the resections with better clinical outcomes contained a higher frequency of mutant cells and thus would have

a higher variant allele fraction (VAF) of the *AKT3* E17K mutation; however, the opposite was true. The VAF of resection 1 was 3%, higher than resection 2 (0%) and resection 3 A (1%). Resection 3P had the highest VAF at 6%, despite only interictal discharges captured from this region. These findings suggest that epileptogenicity does not correlate directly with VAF and there may be non-cell autonomous mechanisms driving epileptogenesis in FCD.

Serial resections had multiple shared protein features

Given the different clinical outcomes following each resection, we next sought to identify cell populations or signaling activity that may explain the observed discrepancies. Fresh tissue from each resection was dissociated into viable single cells for cryopreservation [19]. Cells were thawed and stained with a 43-antibody custom mass cytometry panel encompassing neural lineage and downstream mTOR phosphorylation targets (Supplementary Tables 1 and Supplementary Fig. 2). Samples were barcoded and stained simultaneously for intracellular markers to minimize batch effects. After excluding endothelial and immune cells, we first looked at neural identity profiles. All resections had a similar proportion (41–54%) of β-III-tubulin+ neurons (Fig. 3a upper). In contrast, the second resection had twice the number of GFAP+ astrocytes as resection 1 and there was further expansion in resections 3A and 3P (Fig. 3a lower). Post-surgical astrogliosis likely contributed to the acute change between resections 1 and 2, whereas normal developmental expansion of astrocytes throughout childhood [32] may

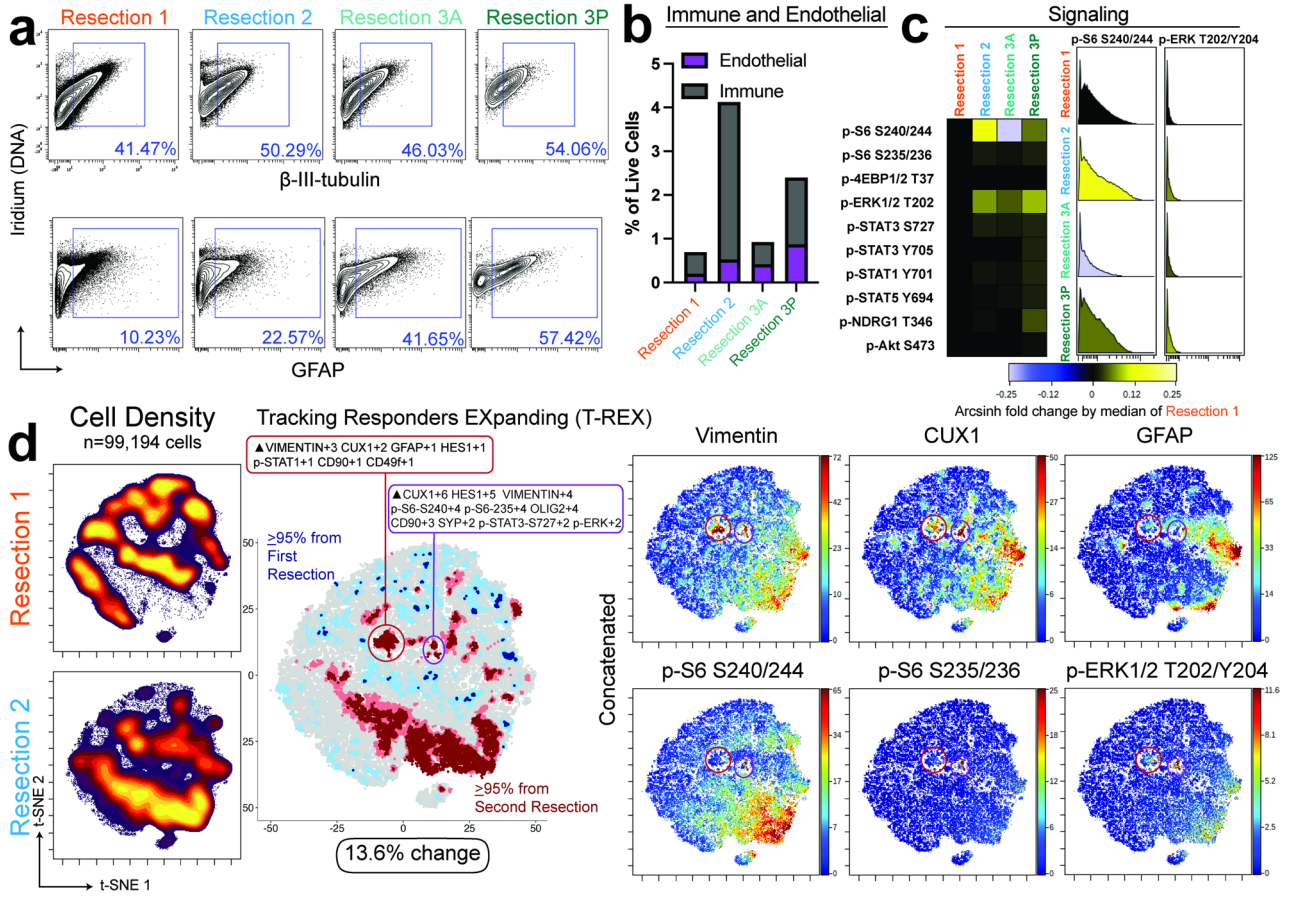

Fig. 3 Mass Cytometry analysis of serial resections reveals shared and diverging features. **a** Biaxial gating depicts the percentage of β-III-tubulin+ neurons (40–51%) band the percentage of GFAP+ astrocytes (10–57%) across resections. **b** Stacked bar graphs depict abundance of immune (grey) and endothelial (purple) cells per resection as a percentage of all live cells analyzed. **c** Heatmap depicting median intensity for signaling readouts across resections, shown relative to resection 1 (left). Histogram overlays show the distribution of per-cell intensity for two example phosphoproteins (right). **d** A t-SNE map was generated with non-immune, non-endothelial cells sampled equally from resections 1 and 2. Density of events from each resection on the shared t-SNE map is shown on the left, with T-REX analysis at right used to identify regions containing events specific to either resections 1 or 2. An overall change of 13.6% (events on the map specific to one resection) was identified. Marker Enrichment Modeling (MEM) was used to generate phenotypic statistical labels for each significant resection-specific cluster. An example of two clusters with their respective MEM labels are depicted along with concatenated heatmaps for selected channels of interest (heatmaps for all channels shown in supplement). The populations of interest are highlighted throughout with dark red and purple circles

account for the higher number of GFAP+ cells in resections 3A and 3P.

To rule out the possibility of post-surgical inflammation as a substantial driver of difference between resections 1 and 2, we performed a focused sub-analysis of immune cells in each resection. There was an expansion of immune cells in resection 2, as expected (Fig. 3b). To statistically compare immune cell subsets, we employed Tracking Responders EXpanding (T-REX) [6], which quantified degree of change by identifying the percentage of phenotypically distinct cells whose presence was > 95% specific to either resection. T-REX is powered to identify rare (1 in 10,000) populations of distinct cells, rendering it particularly valuable in analysis of FCD tissue where only a small population of cells harbor mutations. There was a minimal 6.9% difference between CD45 + CD11b+ immune cells in both resections, with increased p-S6 signaling at both pairs of residues accounting for much of the difference (Supplementary Fig. 3).

Given the central function of mTOR in brain development and cortical dysplasia, our mass cytometry panel was designed to capture multiple readouts of mTOR activity and intersecting pathways (Fig. 3c). Significantly more p-S6$_{S240/244}$ -high cells were observed in all samples compared to other mTOR readouts. In contrast to the concordance between p-S6 residues in immune cells, there was minimal p-S6$_{S235/236}$ signal detected in neural lineage cells. Despite low abundance of other phosphorylation markers across our panel, we were able to capture additional subtle or rare changes in signaling due to our single-cell approach, such as increased levels of p-ERK1/2$_{T202/Y204}$ (Fig. 3c and d).

Seizure-alleviating resections revealed a distinct cell population

We next compared the first two resections, given their proximity in time and disparate seizure outcomes. A t-SNE plot was constructed using 21 cell identity proteins for 49,597 non-immune, non-endothelial cells per sample. T-REX analysis revealed a 69.0% change between resections 1 and 2, with cells falling into three large clusters (Supplementary Fig. 4). Review of individual channel heatmaps revealed S100B and CD90 to be main drivers of the three large clusters within the generated t-SNE map. To refine the analysis and potentially identify rare subsets of cells that were changing across samples, we excluded CD90 and S100B from future t-SNE constructions. Using T-REX, we analysed the new t-SNE construction and identified a 13.6% degree of change across the first and second resections. Marker Enrichment Modeling (MEM) [11] defined protein features enriched in each subset of cells unique to resection 2 (dark red), with two subsets with similar marker protein expression but differential signaling highlighted in Fig. 3d.

To further define cell populations that may account for varying clinical outcomes, we next focused on resections 3 A and 3P. Repeat t-SNE analysis of 8295 non-immune, non-endothelial cells from resections 3 A and 3P revealed a CUX1-high population that clustered separately from other cells (Fig. 4a). The MEM label for this cluster showed these cells were highly enriched for CUX1, HES1, and Vimentin. We confirmed the protein expression identity of these cells through traditional biaxial gating. Next, the Velociraptor algorithm [9] was used to search for the CUX1/HES1/Vimentin cell signature in resections 1 and 2. Cells matching this signature were present at low abundance in both samples (0.20% in resection 1 and 1.04% in resection 2). Notably, the population was more abundant in resections 2 and 3 compared to resection 1, indicating a possible correlation with seizure control. To validate the presence of the CUX1-high cell population in situ, we performed cyclic immunostaining on all four resection tissues. We identified a small subset of cells across all samples that were strongly positive for CUX1 and HES1 and expressed intermediate levels of Vimentin (Fig. 4b and Supplementary Fig. 5).

To confirm that the identified CUX1-high population was not unique to this single FCD patient, we used Velociraptor to search for the identified MEM label in two unrelated cortical malformation cases (MCD2 and MCD3) due to mutations in *NPRL3*, another mTOR pathway gene (see Supplementary Table 3 for clinical characteristics). Both MCD patients had a family history of epilepsy, indicating that the identified *NPRL3* mutations are likely germline. We identified cells with >87% match to the specified MEM label in both samples, with an abundance of 0.29% in MCD2 and 0.74% in MCD3. Thus, we verified that the CUX1-high population was present across distinct patients and correlated with post-operative seizure outcomes.

Discussion

We report here a distinctive FCDIIa case that required multiple surgical resections to improve seizure control. The gain-of-function *AKT3* E17K mutation harbored by our patient has been previously associated with both FCD and hemimegaloencephaly [14, 26]. The recurrence of seizures shortly after the first surgery and need for repeat surgeries is consistent with a reported association between acute postoperative seizures and poor seizure outcomes [30]. The mosaic *AKT3* mutational status in this case provided an opportunity to examine whether mutational burden was associated with seizure severity or abnormal cellular phenotypes. The complicated clinical course of this patient highlights the need for improved phenotyping of seizure-associated cells to

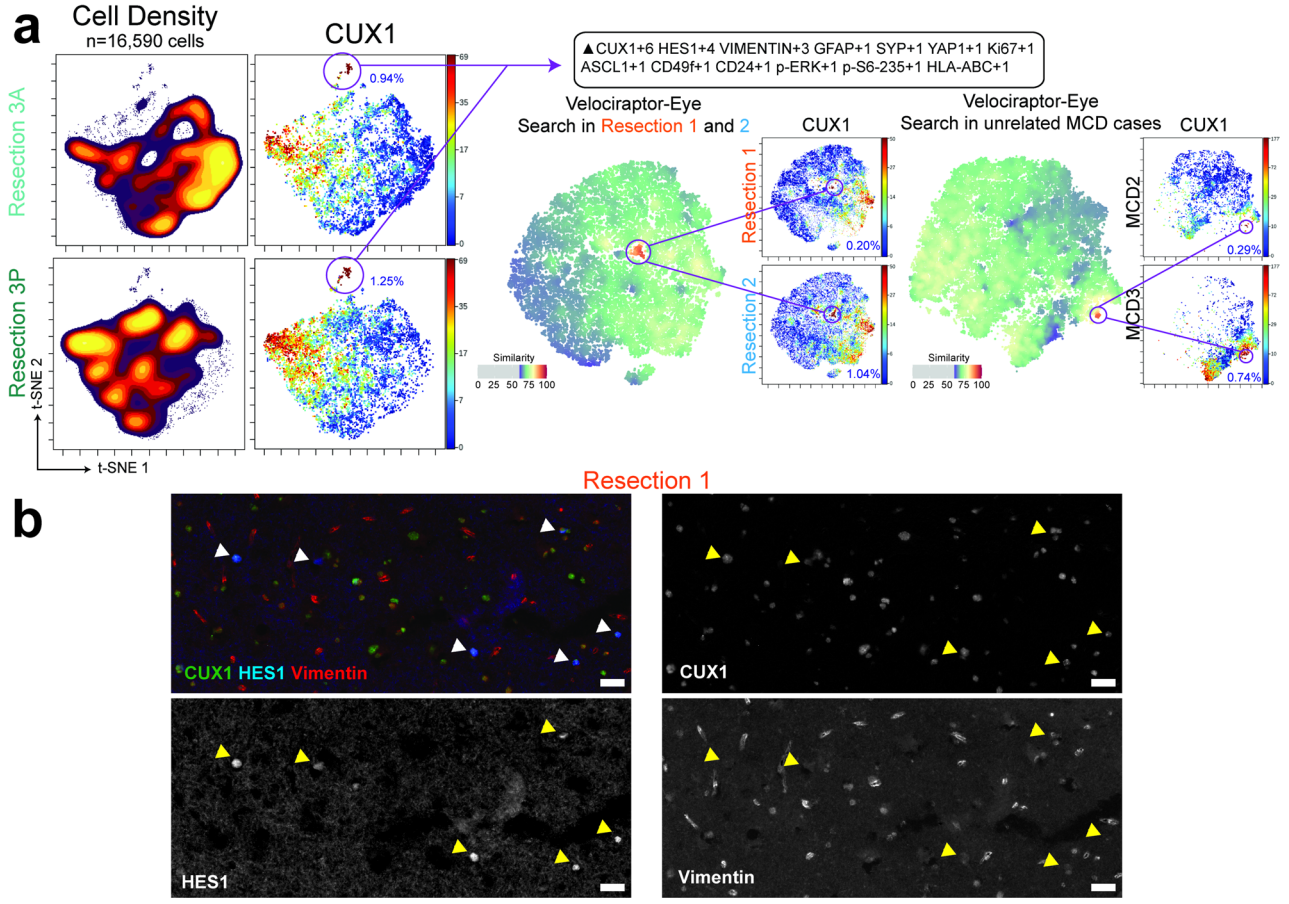

Fig. 4 Targeted search identifies similar CUX1-high cell populations in other FCD cases. **a** A CUX1-high cell population repeatedly clustered separately when performing t-SNE analyses of resections 3 A and 3P (left). A Marker Enrichment Modeling (MEM) label was generated to phenotypically describe this population, which was enriched for CUX1, HES1, and Vimentin. The Velociraptor algorithm [9] was used to search for this MEM label across resections 1 and 2 (center). The population was found in both resections with a > 87% match in MEM label. The population was more abundant in resection 2 versus resection 1. Searching for the same cell signature in 16,724 cells from two unrelated malformation of cortical development (MCD) cases identified a matched population with different abundance across samples (right). **b** Representative images of tri-positive cells with high CUX1 (green)/HES1 (blue), and intermediate Vimentin (red) in resection 1. Arrowheads depict identified cells. Scale bar = 100 µm

minimize invasive surgeries and better understand which cell lineages contribute to seizures.

To examine resected tissues at the protein level, we developed and implemented a custom 43-antibody mass cytometry panel to deeply phenotype tens of thousands of cells per FCD sample. Prior single-cell studies of FCD have focused on transcriptional data with hundreds to thousands of cells per individual [5, 8]. By directly studying protein expression, we bypassed reported discrepancies between human brain transcript and protein expression patterns [7]. Using unsupervised machine learning, we identified a rare (0.2–1.25%) CUX1-high population that was expanded in seizure-alleviating resections and identified a similar phenotype that was present in at least two other MCD cases. Notably, MCD2 experienced a recurrence of seizures one year post-operatively, which may relate to the lower abundance observed of these cells. Additionally, the presence of this cell population across different mutational statuses in FCD1 (somatic) and MCD2/MCD3 (germline) indicates there is likely a disease-specific mechanism at play. CUX1 is expressed in embryonic neural precursors destined to become upper-layer cortical neurons and their mature counterparts [22]. Concordant with these findings, prior work has identified electrical firing abnormalities in upper layer neurons from FCD brain slices [17] and upper layer neuron transcripts, including CUX1, were enriched in individual FCD mutation-positive cells [8]. Collectively, this suggests that this identified population may consist of aberrant cells resembling upper-layer neurons, though intriguingly the protein phenotype is present even when no mutation was detectable. Further studies combining spatial proteomics with targeted mutational sequencing and electrophysiological recordings will help expand on this finding.

A second protein feature that was widely evident in seizure relieving resections, even when *AKT3* VAF was low, was elevated per-cell levels of p-S6$_{S240/244}$. In particular, there was an elevated number of p-S6 signaling events in resection 2 vs. resection 1. Elevation of mTOR activity with no identified mutation in FCD tissue has been reported by multiple groups [14, 25]. This discrepancy may be partially attributed to mTOR activation as a secondary response to seizure activity, independent of etiology [23, 33]. Despite the high levels of p-S6$_{S240/244}$ across samples, there was comparatively minimal p-S6$_{S235/236}$ detected. We and others have shown that there are regional differences in abundance of these two related phosphorylation events, with p-S6$_{S240/244}$ phosphorylation more exclusively depending on mTOR complex activity [15, 29]. Intriguingly, the CUX1-high population identified across resections was an exception to this pattern, displaying high phosphorylation at both pairs of residues on S6 and p-STAT3$_{S727}$ in resections 1 and 2, as well as elevated p-ERK1/2$_{T202/Y204}$ in all four resections. Within immune cells in these tissues, we observed a colinear relationship between both residues, as is often observed in cell lines or other models. Our data suggest that examination of both residues of p-S6 is warranted when analyzing cases of FCD and related mTORopathies, and that elevated mTOR-dependent signaling events are not necessarily directly associated with expression of disease-causing mutations in individual cells.

Examinations of total protein also identified patterns consistent with expectations for the post-surgical environment in the brain. For example, comparison of resections 1 and 2 revealed increased expression of CD90 in the second sample (two-fold higher median intensity on an arcsinh scale). CD90, also known as THY-1, is a neural surface protein that is involved in modulation of neuronal processes [20] and can bind to astrocytic receptors and trigger features of reactive astrocytosis [24]. Thus, the increase in CD90 is most likely explained by astrogliosis secondary to the recent surgery, consistent with the greater abundance of GFAP+ cells in resection 2 versus 1. There was also an expansion of MHC Class I/HLA-ABC expression in seizure-alleviating resections, consistent with prior reports [27].

Comparing mass cytometry data with whole exome sequencing, we identified a discrepancy between mutational burden and seizure outcomes across all four resections. Resection 3P had the highest VAF (6%) despite showing only interictal spikes on ECoG. Resection 2 had no detectable VAF despite seizure freedom for three years and containing a high percentage of cells with active mTOR signaling. Given that 40% of FCDII cases remain unresolved even with > 2000X gene sequencing [4], we posit that this discrepancy is likely due to non-cell autonomous mechanisms driving mTOR activity and/or seizure activity in FCD and not a limitation of sequencing depth. Prior work has identified the presence of dysmorphic neurons in areas with no detectable VAF [25]. In animal models of FCD, neurons proximal to mutation-carrying neurons show hyperactivity [16] and mutated cells can cause migration defects in their neighbors [3]. Recent work has found higher VAF in stereo-EEG electrodes near seizure onset zones in some FCD cases [10]. However, these findings vary widely across patients, indicating that presence of mutant cells may not be the best indicator for clinical outcomes. Additionally, targeted single-cell transcriptional study of FCD revealed aberrations in synaptic transmission genes in non-mutated dysplastic cells [5]. Overall, our findings support the theory that non-cell autonomous mechanisms are contributing to epileptogenesis in FCD.

One limitation of this study is the lack of healthy brain tissue for comparison. Measurement of signaling capacity by suspension mass cytometry requires live cells, which are not routinely available from non-pathogenic brains. Additionally, we cannot definitively state the mutational status of the CUX1-high cells identified given their rarity. Prospective cytometric sorting or high dimensional spatial analyses [2] would provide additional insight into the molecular features of these cells.

Conclusions

In conclusion, our work presents a high dimensional protein-level assessment of a mosaic case of FCD causing drug-refractive epilepsy. We provide evidence for non-cell autonomous mechanisms driving epileptogenesis and highlight a unique cell population that is associated with seizure outcomes. By applying a systematic approach to analyses of serial resections, we present a guide for larger-scale, protein-level studies of FCD to increase understanding of FCD pathogenesis and optimize treatments.

Abbreviations

ECoG	Electrocorticography
FCD	Focal cortical dysplasia
MCD	Malformations of cortical development
MEM	Marker Enrichment Modeling
POD	Postoperative day
Stereo-EEG	Stereotactic EEG
T-REX	Tracking Responders Expanding
VAF	Variant allele fraction

Supplementary Information

The online version contains supplementary material available at https://doi.org/10.1186/s40478-026-02273-3.

Supplementary Material 1.

Acknowledgements
We thank all patients and families who generously donated tissue for this research. We also thank Caroline E. Roe and Claire E. Cross for technical support and helpful discussions on analysis algorithms.

Author contributions
Conceptualization and design of the study: NAE, RAI, KCE. Data Collection: NAE, RPN, BJM, ALA, AMT. Data Analysis: NAE, BJM, AMT, AAB, JMI, RAI, KCE. Writing – original draft: NAE, RAI, KCE. Revision and approval of manuscript: all authors.

Funding
This work was supported by NIH R01NS118580 (RAI, KCE, and JMI), R01CA226833 (JMI), K08NS131572 (ALA), T32GM007347, and T32GM152284. This study was supported in part by the National Institutes of Health P30CA046934 funded Flow Cytometry Shared Resource (RRID: SCR_022035), Human Immunology & Immunotherapy Initiative (S10OD036353), and Research Histology Shared Resource (RRID: SCR_021994) at University of Colorado Anschutz Medical Campus, and the Translational Pathology Shared Resource (NCI/NIH P30CA068485) at Vanderbilt University. We thank the Alvin J. Siteman Cancer Center at Washington University School of Medicine and Barnes-Jewish Hospital in St. Louis, MO. and the Institute of Clinical and Translational Sciences (ICTS) at Washington University in St. Louis, for the use of the Genome Technology Access Center, which provided whole exome sequencing and analysis service. The Siteman Cancer Center is supported in part by an NCI Cancer Center Support Grant #P30 CA091842 and the ICTS is funded by the National Institutes of Health's NCATS Clinical and Translational Science Award (CTSA) program grant #UL1 TR002345.

Data availability
The CyTOF datasets generated and analyzed during the current study are available in the Zenodo repository, https://doi.org/10.5281/zenodo.17833095. All other datasets are available upon reasonable request to the corresponding author.

Declarations

Ethics approval and consent to participate
This study was approved by the Vanderbilt University Institutional Review Board and the Colorado Multiple Institutional Review Board.

Consent for publication
Informed consent/assent was obtained from all patients and guardians included in this study.

Competing interests
The authors declare no competing interests.

Received: 18 December 2025 / Accepted: 27 February 2026
Published online: 13 March 2026

References

1. Abdijadid S, Mathern GW, Levine MS, Cepeda C (2015) Basic Mechanisms of Epileptogenesis in Pediatric Cortical Dysplasia. CNS Neurosci Ther 21:92–103. https://doi.org/10.1111/cns.12345
2. Arceneaux JS, Brockman AA, Khurana R, Chalkley ML, Geben LC, Krbanjevic A, Vestal M, Zafar M, Weatherspoon S, Mobley BC, Ess KC, Ihrie RA (2024) Multiparameter quantitative analyses of diagnostic cells in brain tissues from tuberous sclerosis complex. Cytometry Part B Clin Cytom. https://doi.org/10.1002/cyto.b.22194
3. Baek ST, Copeland B, Yun E-J, Kwon S-K, Guemez-Gamboa A, Schaffer AE, Kim S, Kang H-C, Song S, Mathern GW, Gleeson JG (2015) An AKT3-FOXG1-reelin network underlies defective migration in human focal malformations of cortical development. Nat Med 21:1445–1454. https://doi.org/10.1038/nm.3982
4. Baldassari S, Ribierre T, Marsan E, Adle-Biassette H, Ferrand-Sorbets S, Bulteau C, Dorison N, Fohlen M, Polivka M, Weckhuysen S, Dorfmüller G, Chipaux M, Baulac S (2019) Dissecting the genetic basis of focal cortical dysplasia: a large cohort study. Acta Neuropathol 138:885–900. https://doi.org/10.1007/s00401-019-02061-5
5. Baldassari S, Klingler E, Teijeiro LG, Doladilhe M, Raoux C, Roig-Puiggros S, Bizzotto S, Couturier J, Gilbert A, Sami L, Ribierre T, Aronica E, Adle-Biassette H, Chipaux M, Jabaudon D, Baulac S (2025) Single-cell genotyping and transcriptomic profiling of mosaic focal cortical dysplasia. Nat Neurosci 28:964–972. https://doi.org/10.1038/s41593-025-01936-z
6. Barone SM, Paul AG, Muehling LM, Lannigan JA, Kwok WW, Turner RB, Woodfolk JA, Irish JM (2021) Unsupervised machine learning reveals key immune cell subsets in COVID-19, rhinovirus infection, and cancer therapy. eLife 10:e64653. https://doi.org/10.7554/eLife.64653
7. Bauernfeind AL, Babbitt CC (2017) The predictive nature of transcript expression levels on protein expression in adult human brain. BMC Genomics 18:322. https://doi.org/10.1186/s12864-017-3674-x
8. Bizzotto S, Talukdar M, Stronge EA, Ramirez RB, Yang Y, Huang AY, Hu Q, Hou Y, Hylton NK, Finander B, Tillett A, Zhou Z, Chhouk BH, D'Gama AM, Yang E, Green TE, Reutens DC, Mullen SA, Scheffer IE, Hildebrand MS, Buono RJ, Blümcke I, Poduri AH, Khoshkhoo S, Walsh CA (2025) Cell-type-informed genotyping of mosaic focal epilepsies reveals cell-autonomous and non-cell-autonomous disease-associated transcriptional programs. Proc Natl Acad Sci USA 122:e2509622122. https://doi.org/10.1073/pnas.2509622122
9. Cross CE, Mayeda C, Medina S, Hayes MJ, Kaviany S, Connelly JA, Rathmell JC, Weaver KD, Thompson RC, Chambless LB, Ihrie RA, Irish JM (2024) Velociraptor: cross-platform quantitative search using hallmark cell features
10. D'Gama AM, Phillips HW, Wang Y, Chiu MY, Chahine Y, Swanson AC, Smith RS, Pearl PL, Tsuboyama M, Madsen JR, Lidov H, Lee EA, Prabhu SP, Huang AY, Stone SSD, Walsh CA, Poduri A (2025) Analysis of DNA from brain tissue on stereo-EEG electrodes reveals mosaic epilepsy-related variants. Brain Commun 7:fcaf113. https://doi.org/10.1093/braincomms/fcaf113
11. Diggins KE, Gandelman JS, Roe CE, Irish JM (2018) Generating quantitative cell identity labels with marker enrichment modeling (MEM). CP Cytometry. https://doi.org/10.1002/cpcy.34
12. Galvão IC, Lemoine M, Messias LA, Araújo PAORA, Geraldis JC, Yasuda CL, Alvim MKM, Ghizoni E, Tedeschi H, Cendes F, Rogerio F, Lopes-Cendes I, Veiga DFT (2024) Multimodal single-cell profiling reveals neuronal vulnerability and pathological cell states in focal cortical dysplasia. iScience 27:111337. https://doi.org/10.1016/j.isci.2024.111337
13. Iffland PH, Crino PB (2017) Focal Cortical Dysplasia: Gene Mutations, Cell Signaling, and Therapeutic Implications. Annu Rev Pathol Mech Dis 12:547–571. https://doi.org/10.1146/annurev-pathol-052016-100138
14. Jansen LA, Mirzaa GM, Ishak GE, O'Roak BJ, Hiatt JB, Roden WH, Gunter SA, Christian SL, Collins S, Adams C, Rivière J-B, St-Onge J, Ojemann JG, Shendure J, Hevner RF, Dobyns WB (2015) PI3K/AKT pathway mutations cause a spectrum of brain malformations from megalencephaly to focal cortical dysplasia. Brain 138:1613–1628. https://doi.org/10.1093/brain/awv045
15. Klingebiel M, Dinekov M, Köhler C (2017) Analysis of ribosomal protein S6 baseline phosphorylation and effect of tau pathology in the murine brain and human hippocampus. Brain Res 1659:121–135. https://doi.org/10.1016/j.brainres.2017.01.016
16. Koh HY, Jang J, Ju SH, Kim R, Cho G, Kim DS, Sohn J, Paik S, Lee JH (2021) Non–Cell Autonomous Epileptogenesis in Focal Cortical Dysplasia. Ann Neurol 90:285–299. https://doi.org/10.1002/ana.26149
17. Kushner JK, Hoffman PB, Brzezinski CR, Svalina MN, O'Neill BR, Hankinson TC, Wilkinson CC, Handler MH, Baca SM, Huntsman MM, Alexander AL (2025) Characterizing the diversity of layer 2/3 human neocortical neurons in pediatric epilepsy. eNeuro 12:ENEURO.0247-24.2025. https://doi.org/10.1523/ENEURO.0247-24.2025
18. Lai D, Gade M, Yang E, Koh HY, Lu J, Walley NM, Buckley AF, Sands TT, Akman CI, Mikati MA, McKhann GM, Goldman JE, Canoll P, Alexander AL, Park KL, Von Allmen GK, Rodziyevska O, Bhattacharjee MB, Lidov HGW, Vogel H, Grant GA, Porter BE, Poduri AH, Crino PB, Heinzen EL (2022) Somatic variants in diverse genes leads to a spectrum of focal cortical malformations. Brain 145:2704–2720. https://doi.org/10.1093/brain/awac117
19. Leelatian N, Doxie DB, Greenplate AR, Mobley BC, Lehman JM, Sinnaeve J, Kauffmann RM, Werkhaven JA, Mistry AM, Weaver KD, Thompson RC, Massion PP, Hooks MA, Kelley MC, Chambless LB, Ihrie RA, Irish JM (2017) Single cell analysis of human tissues and solid tumors with mass cytometry. Cytometry Part B Clin 92:68–78. https://doi.org/10.1002/cyto.b.21481
20. Leyton L, Díaz J, Martínez S, Palacios E, Pérez LA, Pérez RD (2019) Thy-1/CD90 a Bidirectional and Lateral Signaling Scaffold. Front Cell Dev Biol 7:132. https://doi.org/10.3389/fcell.2019.00132

21. Najm I, Lal D, Alonso Vanegas M, Cendes F, Lopes-Cendes I, Palmini A, Paglioli E, Sarnat HB, Walsh CA, Wiebe S, Aronica E, Baulac S, Coras R, Kobow K, Cross JH, Garbelli R, Holthausen H, Rössler K, Thom M, El-Osta A, Lee JH, Miyata H, Guerrini R, Piao Y, Zhou D, Blümcke I (2022) The ILAE consensus classification of focal cortical dysplasia: An update proposed by an ad hoc task force of the ILAE diagnostic methods commission. Epilepsia 63:1899–1919. https://doi.org/10.1111/epi.17301
22. Nieto M, Monuki ES, Tang H, Imitola J, Haubst N, Khoury SJ, Cunningham J, Gotz M, Walsh CA (2004) Expression of Cux-1 and Cux-2 in the subventricular zone and upper layers II–IV of the cerebral cortex. J Comp Neurol 479:168–180. https://doi.org/10.1002/cne.20322
23. Okoh J, Mays J, Bacq A, Oses-Prieto JA, Tyanova S, Chen C-J, Imanbeyev K, Doladilhe M, Zhou H, Jafar-Nejad P, Burlingame A, Noebels J, Baulac S, Costa-Mattioli M (2023) Targeted suppression of mTORC2 reduces seizures across models of epilepsy. Nat Commun 14:7364. https://doi.org/10.1038/s41467-023-42922-y
24. Pérez-Núñez R, Chamorro A, González MF, Contreras P, Artigas R, Corvalán AH, Van Zundert B, Reyes C, Moya PR, Avalos AM, Schneider P, Quest AFG, Leyton L (2023) Protein kinase B (AKT) upregulation and Thy-1-αvβ3 integrin-induced phosphorylation of Connexin43 by activated AKT in astrogliosis. J Neuroinflammation 20:5. https://doi.org/10.1186/s12974-022-02677-7
25. Pirozzi F, Berkseth M, Shear R, Gonzalez L, Timms AE, Sulc J, Pao E, Oyama N, Forzano F, Conti V, Guerrini R, Doherty ES, Saitta SC, Lockwood CM, Pritchard CC, Dobyns WB, Novotny E, Wright JNN, Saneto RP, Friedman S, Hauptman J, Ojemann J, Kapur RP, Mirzaa GM (2022) Profiling PI3K-AKT-MTOR variants in focal brain malformations reveals new insights for diagnostic care. Brain 145:925–938. https://doi.org/10.1093/brain/awab376
26. Poduri A, Evrony GD, Cai X, Elhosary PC, Beroukhim R, Lehtinen MK, Hills LB, Heinzen EL, Hill A, Hill RS, Barry BJ, Bourgeois BFD, Riviello JJ, Barkovich AJ, Black PM, Ligon KL, Walsh CA (2012) Somatic Activation of AKT3 Causes Hemispheric Developmental Brain Malformations. Neuron 74:41–48. https://doi.org/10.1016/j.neuron.2012.03.010
27. Prabowo AS, Iyer AM, Anink JJ, Spliet WG, Van Rijen PC, Aronica E (2013) Differential expression of major histocompatibility complex class I in developmental glioneuronal lesions. J Neuroinflammation 10:778. https://doi.org/10.1186/1742-2094-10-12
28. Roe CE, Hayes MJ, Barone SM, Irish JM (2020) Training Novices in Generation and Analysis of High-Dimensional Human Cell Phospho-Flow Cytometry Data. CP Cytometry 93:e71. https://doi.org/10.1002/cpcy.71
29. Rushing GV, Brockman AA, Bollig MK, Leelatian N, Mobley BC, Irish JM, Ess KC, Fu C, Ihrie RA (2019) Location-dependent maintenance of intrinsic susceptibility to mTORC1-driven tumorigenesis. Life Sci Alliance 2:e201800218. https://doi.org/10.26508/lsa.201800218
30. Rylander T, Grubor I, Strandberg MC, Bengzon J (2025) Acute Postoperative Seizures are a Negative Prognostic Factor for Seizure Freedom After Epilepsy Surgery for Focal Cortical Dysplasia. World Neurosurg 202:124352. https://doi.org/10.1016/j.wneu.2025.124352
31. Sim NS, Ko A, Kim WK, Kim SH, Kim JS, Shim K-W, Aronica E, Mijnsbergen C, Spliet WGM, Koh HY, Kim HD, Lee JS, Kim DS, Kang H-C, Lee JH (2019) Precise detection of low-level somatic mutation in resected epilepsy brain tissue. Acta Neuropathol 138:901–912. https://doi.org/10.1007/s00401-019-02052-6
32. Vivi E, Di Benedetto B (2024) Brain stars take the lead during critical periods of early postnatal brain development: relevance of astrocytes in health and mental disorders. Mol Psychiatry 29:2821–2833. https://doi.org/10.1038/s41380-024-02534-4
33. Wong M, Bordey A, Danzer SC (2024) mTOR in acquired and genetic models of epilepsy. In: Noebels JL, Avoli M, Rogawski MA, Vezzani A, Delgado-Escueta AV (eds) Jasper's basic mechanisms of the epilepsies, 5th edn. Oxford University Press, New York, pp 45–74
34. Zhou Y, Song H, Ming G (2024) Genetics of human brain development. Nat Rev Genet 25:26–45. https://doi.org/10.1038/s41576-023-00626-5

Publisher's Note